Electronic Supplementary Information for

A dual-mediator for a sulfur cathode approaching theoretical capacity with low overpotential in aqueous Zn-S batteries

Wanlong Wu,[a] Sibo Wang,[a] Lu Lin,[a] Hua-Yu Shi[a] and Xiaoqi Sun[a,b,*]

[a] Department of Chemistry, Northeastern University, Shenyang 110819, China

[b] National Frontiers Science Center for Industrial Intelligence and Systems Optimization, Northeastern University, Shenyang 110819, China

*E-mail: sunxiaoqi@mail.neu.edu.cn

Methods

Materials: Graphite foil was purchased from SGL group (Germany). Sulfur and sodium alginate were purchased from Sinopharm Chemical Reagent Co. Ltd. Ketjen black (KB) was purchased from Lion Specialty Chemicals (Japan). Glass fiber separators were purchased from Merck Millipore Ltd. The other reagents were obtained from Aladdin Chemical Reagent Co. Ltd.

Preparation of S/KB composite: Sulfur and KB were mixed at a weight ratio of 5:4 and heated at 155 °C for 10 h.

Characterizations: The morphologies were characterized by a scanning electron microscope on HITACHI, SU8010, Japan. The nitrogen adsorption and desorption isotherms were obtained at 77.3 K on an ASAP 2460 (Micromeritics) volumetric adsorption analyze. The surface area was calculated using the Brunauer-Emmett-Teller (BET) method. The pore size distribution curves were collected by the DFT method using the adsorption branch isotherm. TGA was performed on Ruigaku TG/DTA8122 (Japan) from 30 to 500 °C with a heating rate of 10 °C min^{-1} in air atmosphere. XPS was conducted on KRATOS, Axis Ultra ^{DLD} (UK) with Al-Kα radiation as the excitation source. The data was analyzed using CasaXPS software and calibrated by referencing the C 1s peak to 284.6 eV. In-situ Raman analysis of sulfur cathode was carried out on BWS465-532S, B&W Tek Inc., and the Raman spectra of electrolytes were obtained on HORIBA (JOBIN YVON French). TEM images were obtained on a FEI Talos F200X G2 transmission electron microscope. UV-Vis spectra were collected by a Lambda XLS+ UV-Vis spectrometer. XRD was conducted on a PANalytical Empyrean diffractometer with Cu Kα radiation.

Electrochemical measurements: The electrodes were prepared by mixing S/KB and the sodium alginate binder at a mass ratio of 9:1 in water to form slurry (5:4:1 ratio of S:KB:binder). The slurry was casted onto graphite foil substrate and dried at room temperature. The mass loading of sulfur was around 3 mg cm^{-2} for regular tests or 5.1 mg cm^{-2} for high sulfur loading tests. Two electrode Swagelok® type cells were assembled with sulfur cathode, Zn anode, and glass fiber separators. The cell body was composed of Teflon, and titanium rods were used as the current collectors. The area of separators, sulfur cathode and Zn anode was 1.13 cm^{-2}. The thickness of separator was 0.12 mm. The thickness of sulfur cathode was 0.22 mm and 0.43 mm for 3 mg cm^{-2} and 5.1 mg cm^{-2} loadings, respectively. The thickness/mass of Zn anode was 0.13 mm/110 mg for excess anode tests, and 0.02 mm/12 mg for N/P = 2 tests. The discharge using 0.25 m $R_4N^+Cl^-$ electrolyte was carried out in T-shaped Swagelok® three electrode cells with sulfur, Ti and SCE as the working, counter and reference electrodes. The electrochemical measurements were performed on Bio-logic VMP3 or LANHE CT2001A electrochemical system.

Computational details: All quantum chemical calculations, including geometry optimizations and frequency calculations, were performed at the B3LYP/6-31G* level with Gaussian 16. MD simulations were carried out with the Materials Studio software. The box size was 57× 57 ×57 nm^3. The molar ratio of $Zn(OAc)_2$, $Me_3PhN^+I^-$, and H_2O was 1 : 0.25 : 55.56, which agreed with the electrolyte concentrations. NVT was performed at a constant temperature of 298 K for 50 ps to ensure the equilibrium state, and NPT running for 50 ps with ordinary pressure was applied to study the properties of the structure.

Supplementary Figures

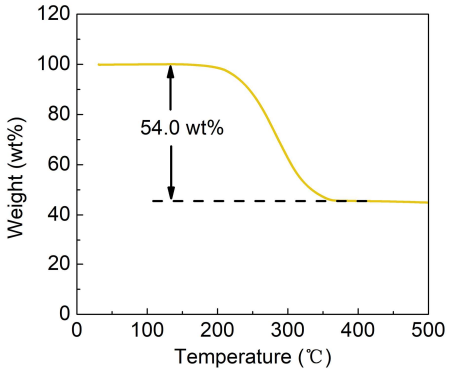

Figure S1. TGA curve of S/KB composite material.

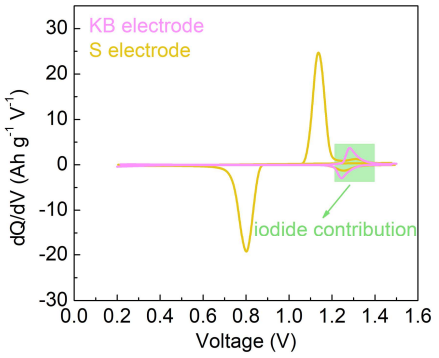

Figure S2. Differential capacity curves of KB and sulfur cathodes in the $Zn(OAc)_2/Me_3PhN^+I^-$ electrolyte.

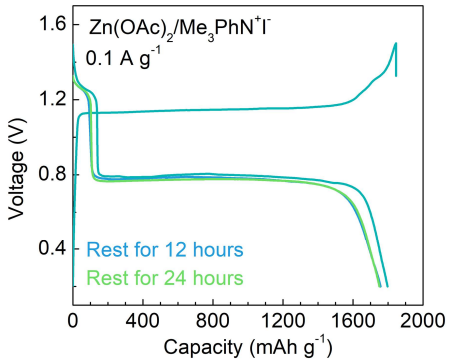

Figure S3. Self-discharge behavior of Zn-S cell in the $Zn(OAc)_2/Me_3PhN^+I^-$ electrolyte.

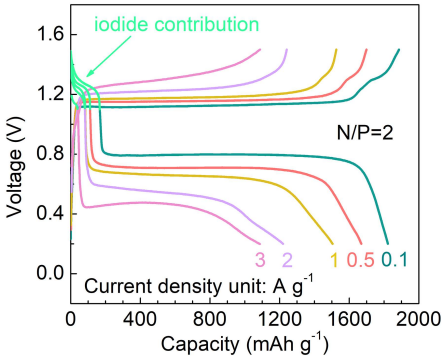

Figure S4. Charge/discharge curves in the $Zn(OAc)_2/Me_3PhN^+I^-$ electrolyte at different current densities with limited anode of N/P=2.

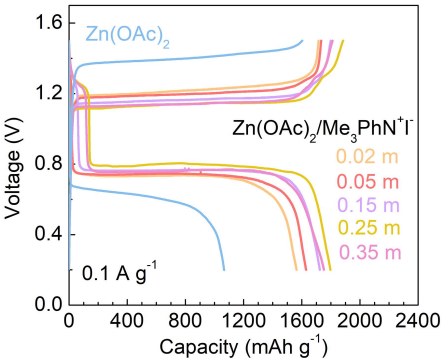

Figure S5. Charge/discharge curves in the $Zn(OAc)_2$ and $Zn(OAc)_2/Me_3PhN^+I^-$ electrolytes with different concentrations of $Me_3PhN^+I^-$ at 0.1 A g^{-1}. With the introduction of 0.02 m $Me_3PhN^+I^-$, the sulfur cathode presents 1564 mAh g^{-1} capacity with 0.49 V overpotential, which is superior to 1066 mAh g^{-1} capacity and 0.75 V overpotential obtained with the benchmark $Zn(OAc)_2$ electrolyte. The performance further enhances with the increase of concentration to 0.25 m. With 0.35 m $Me_3PhN^+I^-$, however, both capacity and overpotential degrades in comparison to 0.25 m $Me_3PhN^+I^-$. The results suggest that 0.25 m is the optimal $Me_3PhN^+I^-$ concentration and is therefore applied.

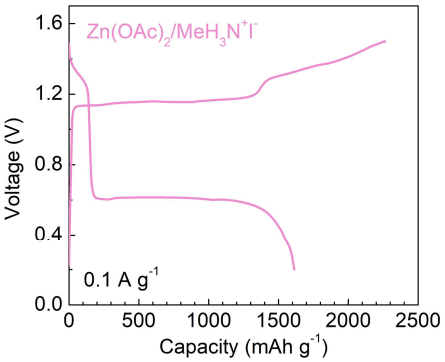

Figure S6. Charge/discharge curves of Zn-S cells at 0.1 A g^{-1} in the $Zn(OAc)_2/MeH_3N^+I^-$ electrolyte.

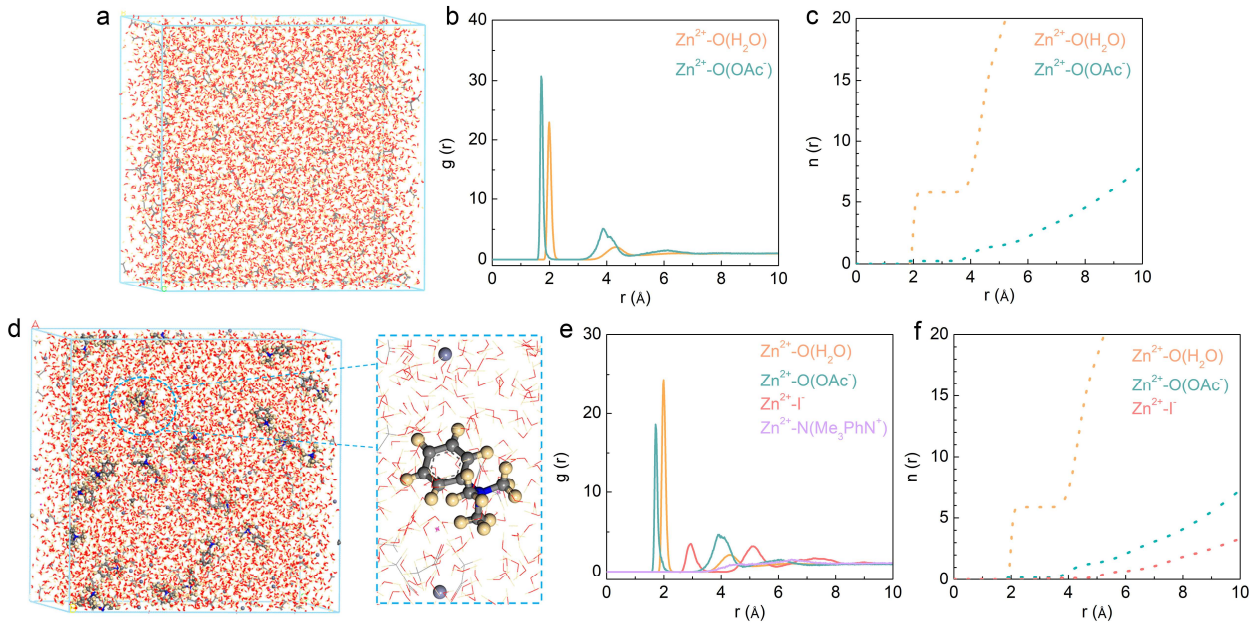

Figure S7. (a,d) Snapshots of the MD simulation cells, (b,e) the resulting RDFs and (c,f) coordination numbers in the (a-c) $Zn(OAc)_2$ and (d-f) $Zn(OAc)_2$/$Me_3PhN^+I^-$electrolytes. In $Zn(OAc)_2$, the first solvation shell of Zn^{2+} is mainly composed of H_2O with a distance of 2.0 Å, and the entrance of OAc^- (at 1.7 Å) is very little. The second solvation shell containing H_2O and OAc^- is found at around 4 Å. After adding $Me_3PhN^+I^-$, these structures stay almost the same. Besides, the I^- content in the first solvation shell of Zn^{2+} is negligible, and the distances between Zn^{2+} and Me_3PhN^+ are above 6 Å. The results suggest that $Me_3PhN^+I^-$ has little influence on the solvation structure of Zn^{2+} in the electrolyte.

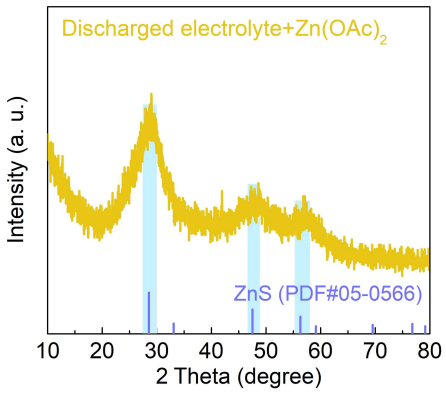

Figure S8. XRD pattern of the precipitate formed by adding $Zn(OAc)_2$ solution to the $Me_4N^+Cl^-$ electrolyte after discharge of sulfur electrode.

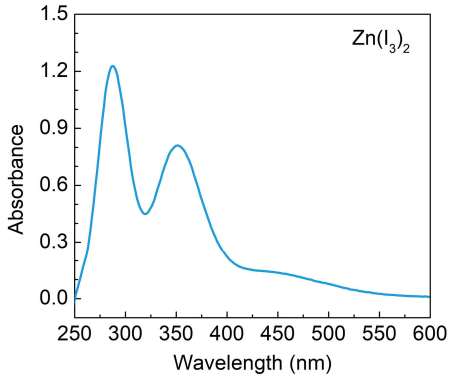

Figure S9. UV-Vis spectrum of the 100 times diluent of saturated $Zn(I_3)_2$ solution.

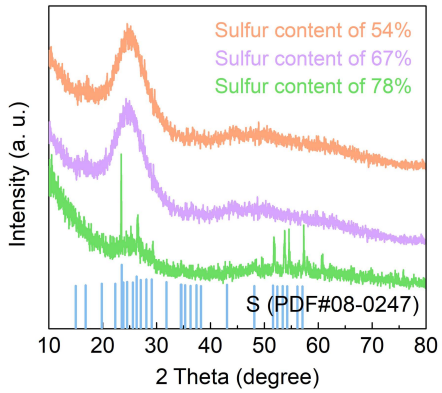

Figure S10. XRD patterns of S/KB with the different sulfur content. Diffraction peaks are observed with the sulfur content of 78%, which are indexed to the S phase (PDF#08-0247). With the sulfur content of 54% and 67%, on the other hand, those peaks diminish. Considering the increased content of KB in these latter cases, more nucleation sites are provided for S during the cooling process of melt diffusion. The resulting solid thus lacks long-rang crystal ordering and does not show diffraction peaks. Nevertheless, the short-range lattice spacings of S can be identified in the HR-TEM image (Figure 1c).

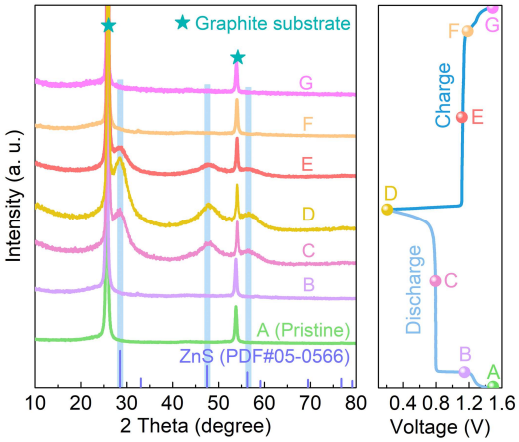

Figure S11. Ex-situ XRD patterns of sulfur cathode at the different states in the $Zn(OAc)_2/Me_3PhN^+I^-$ electrolyte.

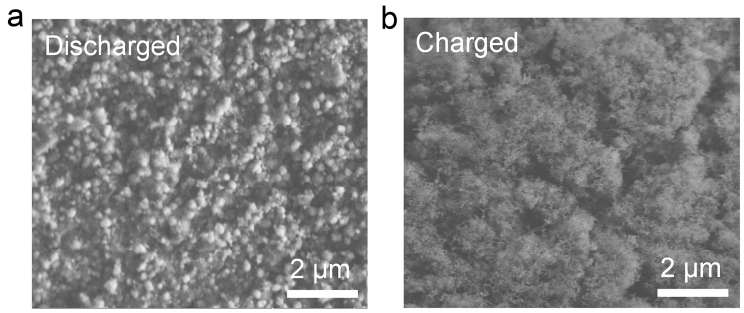

Figure S12. SEM images of the (a) discharged and (b) charged sulfur cathode in the $Zn(OAc)_2/Me_3PhN^+I^-$ electrolyte.

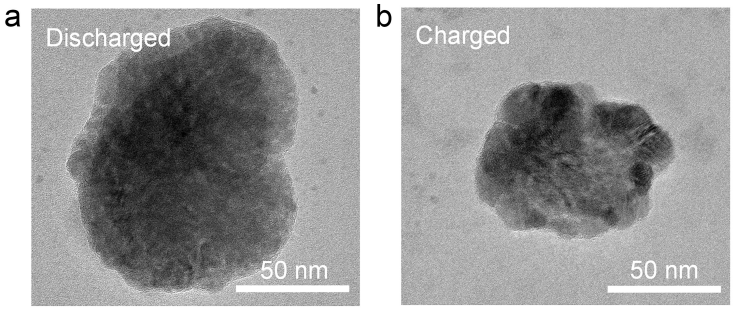

Figure S13. TEM images of the (a) discharged and (b) charged sulfur cathode in the $Zn(OAc)_2/Me_3PhN^+I^-$ electrolyte.